Dalton Transactions

ROYAL SOCIETY OF CHEMISTRY

PAPER

View Article Online
View Journal | View Issue

Cite this: *Dalton Trans.*, 2022, **51**, 15458

$Cd[B_2(SO_4)_4]$ and $H_2[B_2(SO_4)_4]$ – a phyllosilicate-analogous borosulfate and its homeotypic heteropolyacid†

Matthias Hämmer, [a] Leonard C. Pasqualini, [b] Sean S. Sebastian, [c] Hubert Huppertz, [b] Henning A. Höppe *[a] and Jörn Bruns *[c]

Received 19th July 2022,
Accepted 10th September 2022

DOI: 10.1039/d2dt02344j

rsc.li/dalton

Borosulfates consist of heteropolyanionic networks of corner-shared (SO_4)- and (BO_4)-tetrahedra charge compensated by metal or non-metal cations. The anionic substructures differ significantly, depending on the different branching of the silicate-analogous borosulfate building blocks. However, only one acid has been characterized by single crystal X-ray diffraction so far. Herein, we present $H_2[B_2(SO_4)_4]$ as the first phyllosilicate analogue representative, together with the homeotypic representative $Cd[B_2(SO_4)_4]$. The latter can be considered the cadmium salt of the former. Their crystal structures and crystallographic relationship are elucidated. For $H_2[B_2(SO_4)_4]$, the bonding situation is examined using Hirshfeld-surface analysis. Further, the optical and thermal properties of $Cd[B_2(SO_4)_4]$ are investigated by FTIR and UV-Vis spectroscopy, thermogravimetry, as well as temperature-programmed powder X-ray diffraction.

Introduction

In recent years, interest in borosulfates has been growing steadily, not only due to their structural versatility[1] but also for their potential applications in the fields of solid acid electrolytes and SHG materials.[2–4] The anionic substructures of borosulfates are similar to silicates and consist – except for rare cases[4–6] – of (SO_4)- and (BO_4)-tetrahedra connected *via* one common vertex. Accordingly, oligomeric anions like in $K_5[B(SO_4)_4]$,[7] which was the first reported representative, anionic chains[8–15] and layers[16–18] as well as extended 3D network structures[2,8] have been presented. In contrast to alumosilicates, where Al–O–Al bonds are unexpected according to Loewenstein's rule[19] and in violation of Pauling's rules,[20] several so-called unconventional borosulfates with B–O–B[15,21–24] and even S–O–S[8,11,25–27] bridges are known. Hitherto, borosulfates with anionic chains are particularly numerous, whereas 3D networks are especially scarce. In contrast to the structural diversity of the anionic substructure, which is expected to be growing even bigger, the nature of the charge-compensating cations is so far limited. Although, compounds with cations of different valence (monovalent up to trivalent) are known, apart from ammonium,[9] oxonium,[2,11] and two heteropolycationic Au–Cl species[28] the cations are only monoatomic. Considering the special segment of the conventional borosulfates with phyllosilicate-analogous topology, *i.e.* with infinite two dimensional heteropolyanions, only structures with divalent cations have been reported so far. They generally follow the composition $M[B_2(SO_4)_4]$ with M = Mg^{2+},[15] Ca^{2+},[29] Co^{2+},[17,18] Ni^{2+},[17] Zn^{2+},[30] Mn^{2+},[30] Cu^{2+}.[31] All of these compounds share the structural motif of connected zwölfer and vierer rings, consisting of alternating (BO_4)- and (SO_4)-tetrahedra as their heteropolyanion. This set of compounds can be grouped by the adapted crystal structure differing in the location of the cations in the structure. They are located either within the zwölfer ring of the anionic layer (Mg^{2+}, Mn^{2+}, Co^{2+}, Zn^{2+}, Cu^{2+}) or between adjacent layers (Mg^{2+}, Ni^{2+}, Ca^{2+}, Co^{2+}). All cations are octahedrally coordinated, with $Ca[B_2(SO_4)_4]$ as the only exception (CN = 8) crystallizing in an own structure type. There are two structure types for the "cation within layer" variant, namely $Zn[B_2(SO_4)_4]$ and $Mn[B_2(SO_4)_4]$ differing merely in the orientation of one (SO_4)-tetrahedron. The "cation between layer" compounds crystallize in the α-$Mg[B_2(SO_4)_4]$ structure type. Polymorphism between these two variants is reported for $M[B_2(SO_4)_4]$ (M = Mg^{2+}, Co^{2+}).[15,17,18] Moreover, $H[B(SO_4)(S_2O_7)]$ is the only acid with reported crystal structure in the material class of borosulfates, so far.[11] In general, borosulfates can be considered to be salts of the superacid $HB(HSO_4)_4$.[32]

Herein, we present the syntheses and crystal structures of two novel phyllosilicate-analogous borosulfates, namely the

[a]*Institute of Physics, University Augsburg, Universitätsstraße 1, 86159 Augsburg, Germany*
[b]*Institute of General, Inorganic and Theoretical Chemistry, University of Innsbruck, Innrain 80-82, 6020 Innsbruck, Austria*
[c]*Institute of Inorganic Chemistry, University of Cologne, Greinstraße 6, 50939 Cologne, Germany. E-mail: j.bruns@uni-koeln.de*

†Electronic supplementary information (ESI) available. CCDC 2207483, 2176209 and 2171676. For ESI and crystallographic data in CIF or other electronic format see DOI: https://doi.org/10.1039/d2dt02344j

heteropolyacid $H_2[B_2(SO_4)_4]$ and the homeotypic $Cd[B_2(SO_4)_4]$. The latter was postulated by Schott and Kibbel as early as 1962 based on gravimetry and acidimetric titration.[33] Herein, this compound's crystal structure and its optical and thermal properties are addressed. Coevally, a more detailed study of the complex thermal decomposition behaviour of $Cd[B_2(SO_4)_4]$ is reported along with the two unconventional borosulfates $Cd[B_2O(SO_4)_3]$ and $Cd_4[B_2O(SO_4)_6]$.

Results and discussion

Syntheses

Both compounds were prepared solvothermally.

$H_2[B_2(SO_4)_4]$ was synthesized starting from H_3BO_3 and liquid SO_3. For the exact titration of the latter, a specially designed apparatus is needed. It is detailed in the Experimental section. The starting materials were filled into a glass ampoule, which was subsequently sealed under reduced pressure and heat treated at 390 K. A white solid including several colourless single crystals was obtained (Fig. S1†). The utilization of the specially designed apparatus and titration of the exact amount of SO_3 (0.4 ml for 200 mg H_3BO_3) appears to be crucial for the successful synthesis. By lowering the amount of SO_3 by only 0.1 ml, a colourless and highly viscous liquid is obtained, what we were able to show reproducibly (Fig. S2†). The liquid cannot be crystallized at reduced temperature. Crystals of $H_2[B_2(SO_4)_4]$ are extremely hygroscopic. Furthermore, the solid sample reacts easily with a polyacetate foil (Fig. S3†). Consequently, no characterization beyond single-crystal XRD could be performed.

$Cd[B_2(SO_4)_4]$ can be obtained *via* two different synthetic routes (**I** and **II**), both employing solvothermal syntheses starting from CdO, H_3BO_3 or B_2O_3 and oleum (65% SO_3). The starting materials were filled into glass ampoules, which were subsequently sealed, and heat treated at 523 K and 573 K, respectively. *Via* both routes, colourless powders containing large single crystals were obtained (Fig. S4†). Phase-purity was confirmed by powder X-ray (PXRD) diffraction and Rietveld refinement in both cases (Fig. S5, S6 and Table S1†). Noteworthy, no indication for synthesis dependent polymorphism was observed during these syntheses despite synthesis variations such as furnace temperature, SO_3 content and aging – in contrast to the other transition metal borosulfates discussed in the Introduction.

Crystal structures

$H_2[B_2(SO_4)_4]$. The heteropolyacid $H_2[B_2(SO_4)_4]$ crystallizes in a new structure type in the triclinic crystal system with space group $P\bar{1}$ (no. 2) and two formula units per unit cell (Fig. 1). Crystallographic details, bond lengths and angles can be found in Tables S2–S7.† The asymmetric unit of $H_2[B_2(SO_4)_4]$ consists of four crystallographically independent (SO_4)- and two (BO_4)-tetrahedra (Fig. S7†). These are connected *via* common corners with alternating B–O–S bonds. All (BO_4)-tetrahedra share four vertices with one (SO_4)-tetrahedron. They

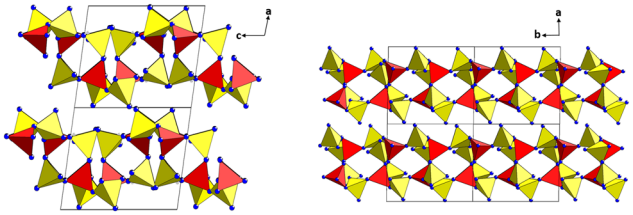

Fig. 1 Phyllosilicate analogue topology in the structure of $H_2[B_2(SO_4)_4]$. Hydrogen bonding occurs only within the layers and not in between the layers. Left: quadruple cell parallel to the crystallographic *b*-axis; right: quadruple parallel to the crystallographic *c*-axis; red tetrahedra – (BO_4), yellow tetrahedra – (SO_4).

form phyllosilicate-analogous layers comprising zwölfer and vierer rings and resembling the structural motive introduced before (Fig. 1 and 2). Two of the (SO_4)-tetrahedra exhibit significantly elongated terminal S–O bonds (S1–O1 149.78(8) and S3–O10 149.69(7) pm) which carry the hydrogen atoms, countering the charge of the heteropolyanion. From a strict ionic point of view, the crystal structure can be considered to consist of the borosulfate anion charge balanced by protons. Strong to moderately strong intra-layer hydrogen bonds are formed to adjacent (SO_4)-tetrahedra with donor–acceptor distances of 249.1(1) and 250.1(1) pm (Table S7†).[35] These may be considered a major cause for the distortion of the zwölfer rings in

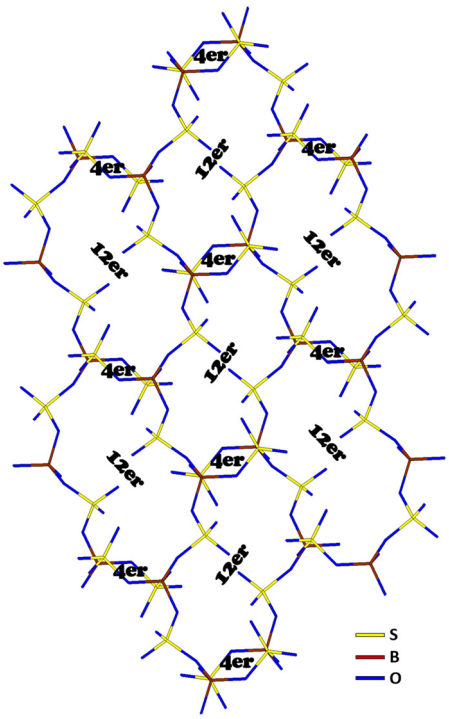

Fig. 2 Cut-out of the layers found for the structure of $H_2[B_2(SO_4)_4]$ depicted in a wire and sticks model. Hydrogen atoms and respective bonds are omitted. The structure exhibits zwölfer- and vierer-rings (abbreviated as 12er and 4er) of corner-linked (SO_4)- and (BO_4)-tetrahedra.

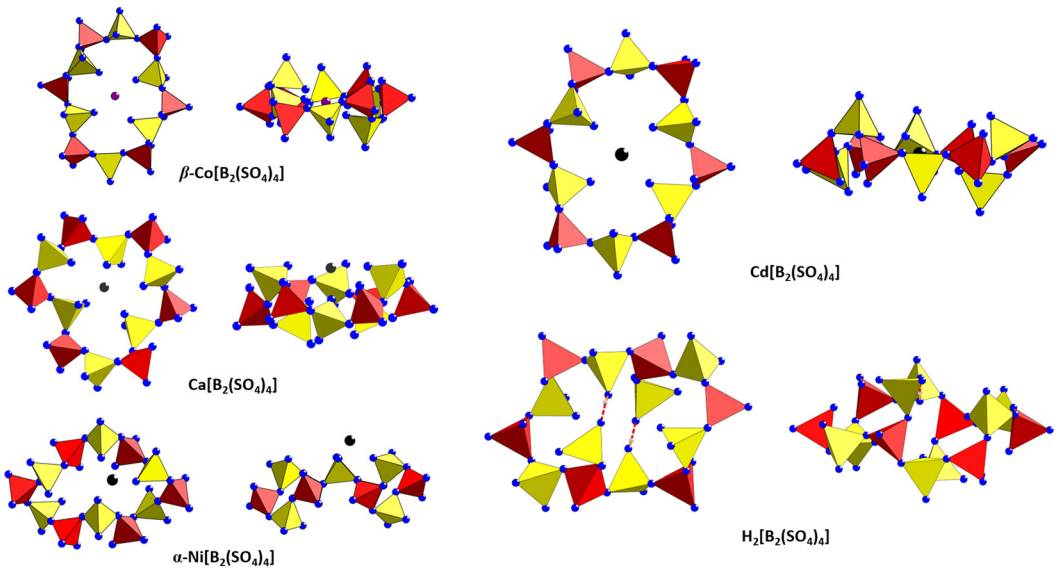

Fig. 3 Location of the cations in the structures of phyllosilicate-analogous borosulfates; red tetrahedra – (BO_4), yellow tetrahedra – (SO_4).

contrast to the homeotypic transition metal borosulfates (Fig. 3). Consequently, the stacking of the layers occurs only *via* van der Waals interactions.

The deviations from tetrahedral symmetry were calculated using the method of Balić-Žunić and Makovicky based on all ligands enclosing spheres on experimental data.[36,37] All (BO_4)- and (SO_4)-tetrahedra can be considered regular[38] with deviations between 0.2% and 0.3%.

$Cd[B_2(SO_4)_4]$. $Cd[B_2(SO_4)_4]$ crystallizes in the $Mn[B_2(SO_4)_4]$ structure type[30] in the monoclinic crystal system with space group $P2_1/n$ (no. 14) and two formula units per unit cell (Fig. 4 and S8†). Crystallographic details, bond lengths and angles can be found in Tables S8–S13 and Fig. S8.† As for $H_2[B_2(SO_4)_4]$, the borosulfate anion of $Cd[B_2(SO_4)_4]$ forms $B(SO_4)_4$ supertetrahedra exhibiting exclusively alternating B–O–S bonds. The supertetrahedra share alternately edges and corners forming sechser rings (Fig. S9†). Consequently, the anion can be classified as phyllosilicate-analogous. More precisely, the anion can be described by the Niggli formula $^2_\infty\{[B(SO_4)_{2/2}{}^e(SO_4)_{2/2}{}^c]^-\}$ (e = edge sharing, c = corner sharing) by considering the supertetrahedron $B(SO_4)_4$ as building unit. Regarding the individual tetrahedra, the layers comprise zwölfer and vierer rings. Each zwölfer ring is connected to four other zwölfer rings directly and to another two *via* vierer rings. The silicate-analogy can be demonstrated by the comparison to the mineral manganpyrosmalite comprising an anionic substructure formed by zwölfer and vierer rings as well as additional sechser rings.[39] So far, no anion exhibting exclusively zwölfer and vierer rings has been observed for the class of silicates. The cadmium cation in $Cd[B_2(SO_4)_4]$ is octahedrally coordinated by six oxygen atoms, *i.e.* monodentately by six (SO_4)-tetrahedra (Fig. 5). Four (SO_4)-tetrahedra belong to an anionic layer with the cation residing inside the zwölfer ring whereas the remaining two belong to the layers above and below, respectively.

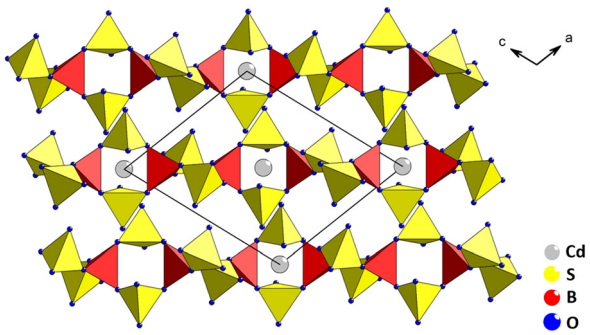

Fig. 4 Unit cell of $Cd[B_2(SO_4)_4]$ viewed along [010].

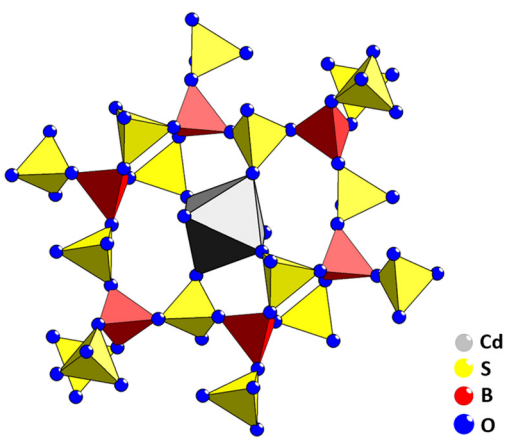

Fig. 5 Octahedral coordination environment of the cadmium cations in $Cd[B_2(SO_4)_4]$ and the location in the zwölfer ring; the two additional oxygen atoms belong to the anion layers above and below, respectively.

In contrast to $H_2[B_2(SO_4)_4]$, the asymmetric unit of $Cd[B_2(SO_4)_4]$ comprises only two crystallographically independent (SO_4)-tetrahedra and one (BO_4)-tetrahedron as well as one CdO_6 octahedron (Fig. S8†). According to calculations by the method of Balić-Žunić and Makovicky, the (BO_4)- and (SO_4)-tetrahedra can all be classified as regular with deviations from the tetrahedral symmetry of 0.5%, 0.1% and 0.6% for $B1O_4$, $S1O_4$ and $S2O_4$, respectively. The Cd–O distances ranging from 222.9(3) to 230.0(2) pm are reasonably close to the sum of ionic radii (220 pm).[40] The deviation from the octahedral symmetry amounts to 6.1%. This value differs insignificantly from isotypic $Mn[B_2(SO_4)_4]$ (Δ_{octa} = 7.9%) or homeotypic $Zn[B_2(SO_4)_4]$ (Δ_{octa} = 5.8%).

On a more general note, $Cd[B_2(SO_4)_4]$ crystallizes in the $Mn[B_2(SO_4)_4]$ structure type. As introduced before, there is the homeotypic $Zn[B_2(SO_4)_4]$ structure type also exhibiting "cations within layer" configuration (Fig. 3). The latter is also adapted by β-$Mg[B_2(SO_4)_4]$, β-$Co[B_2(SO_4)_4]$ and β-$Ni[B_2(SO_4)_4]$,[41] while the only further example for the former structure type is β-$Cu[B_2(SO_4)_4]$. A trend can be found by comparing the acidity of the respective binary oxides. According to the Lux–Flood concept, these borosulfates can be considered to be combinations of the strong acids SO_3 and B_2O_3 and the basic transition metal oxides (*i.e.* CdO, MnO, ZnO, MgO, CoO, NiO, CuO).[42] When excluding the copper representative due to the dominant Jahn–Teller distortion in this compound, the $Mn[B_2(SO_4)_4]$ structure type appears to be adapted for the stronger bases MnO and CdO, while the $Zn[B_2(SO_4)_4]$ structure type is adapted for the slightly weaker remaining bases. Remarkably, polymorphism with "cation between layer" and "cation within layer" polymorphs was only observed by experiment for the latter structure type, so far.

Crystallographic relationship

Chemically, $Cd[B_2(SO_4)_4]$ can be considered the metal salt of the heteropolyacid $H_2[B_2(SO_4)_4]$. This and the topological relationship is obvious when comparing the sum formulae and the layers consisting of zwölfer and vierer rings (Fig. 3). Moreover, $H_2[B_2(SO_4)_4]$ may be considered as the free acid form of all the phyllosilicate-analogous transition metal borosulfates. Although both space groups as well as the unit cell sizes suggest a direct group–subgroup relationship of index t2 according to a Bärnighausen scheme, the distortion of both crystal structures, *i.e.* of $Cd[B_2(SO_4)_4]$ and $H_2[B_2(SO_4)_4]$, with respect to each other is too significant to be subject to such a close relationship – an essence of the respective distortions of the anion despite the same topology is shown in Fig. S10.†

Electrostatic calculations and continuous shape measures

The electrostatic reasonability of the crystal structures of $H_2[B_2(SO_4)_4]$ and $Cd[B_2(SO_4)_4]$ and all coordination numbers were confirmed by calculations based on the MAPLE (MAdelung Part of Lattice Energy) concept (Tables S14†).[43–46] These calculations yielded analogous effective coordination numbers for $Cd[B_2(SO_4)_4]$ as for the isotypic and homeotypic compounds (Tables S15 and S16†).

In Table S17† the Continuous Shape Measure (CShM) values[47] for the coordination polyhedra of the non-oxygen atoms within the asymmetric units of all currently known phyllosilicate-analogous borosulfates are summarized. The CShM values were calculated using the algorithm developed by Casanova *et al.* using the Shape 2.1 program.[48]

Hirshfeld-surface analysis

In order to visualize the non-covalent interactions (NCIs) within the network of the free acid $H_2[B_2(SO_4)_4]$, Hirshfeld-surfaces and fingerprint plots are utilized.[49,50] The Hirshfeld-surface is the isosurface where the ratio of the spherically averaged electron densities of atoms inside the surface (the promolecule) and all atoms in the structure is equal to 0.5.[49] Two values, the distances to the closest atom on the interior (d_i) and the exterior (d_e), are associated to every point on the surface. In this work, we exclusively show d_{norm} mapped onto the surfaces, which is given by:

$$d_{norm} = \frac{(d_i - r_i^{vdW})}{r_i^{vdW}} + \frac{(d_e - r_e^{vdW})}{r_e^{vdW}}$$

where r_i^{vdW} and r_e^{vdW} are the van der Waals-radii of the respective atoms. The surface is then coloured with a gradient from red (negative d_{norm} values, *i.e.* close contacts) over white (d_{norm} is equal to zero, *i.e.* exact van der Waals-radii) to blue (positive d_{norm} values, weak interactions). The fingerprint plots are a scatterplot of d_e *vs.* d_i for all points on a Hirshfeld-surface and may be used to identify strong interactions as spikes directed to the origin of the plot.

The Hirshfeld-surface around one zwölfer ring displays – in line with the crystal structure description before – the lack of strong interactions between the layers (Fig. S11 and S12†). Any hydrogen bonding is strictly confined to the inside of the layer and accounts for 22.9% of the surface of one zwölfer ring (Fig. 6). The associated fingerprint plot displays three distinct spikes corresponding to the O–B and O–S contacts (covalent bonds) within the layers as well as the donor/acceptor-pairs of the hydrogen bridges within the layers. The large green area in the full fingerprint plot corresponds to the van der Waals contacts of the zwölfer ring to the adjacent layers.

The morphology and mapping on the Hirshfeld-surfaces around the two hydrogen atoms in the structure shows that the hydrogen bridges occur exclusively within the same layer (Fig. 7). This is in contrast to all hitherto known phyllosilicate-analogous borosulfates. There, the cations inside the rings are always coordinated by oxygen atoms of the adjacent layers – either two or three layers contribute to the cation's coordination in the "cation between layers" and "cation within layers" configurations, respectively. This lack of inter-layer bonding might explain the observed extraordinary reactivity of the compound.

Optical properties

Infrared spectroscopy. The infrared spectrum of $Cd[B_2(SO_4)_4]$ is shown in Fig. S13.† The spectrum resembles those of isotypic β-$Cu[B_2(SO_4)_4]$, homeotypic α-$Co[B_2(SO_4)_4]$

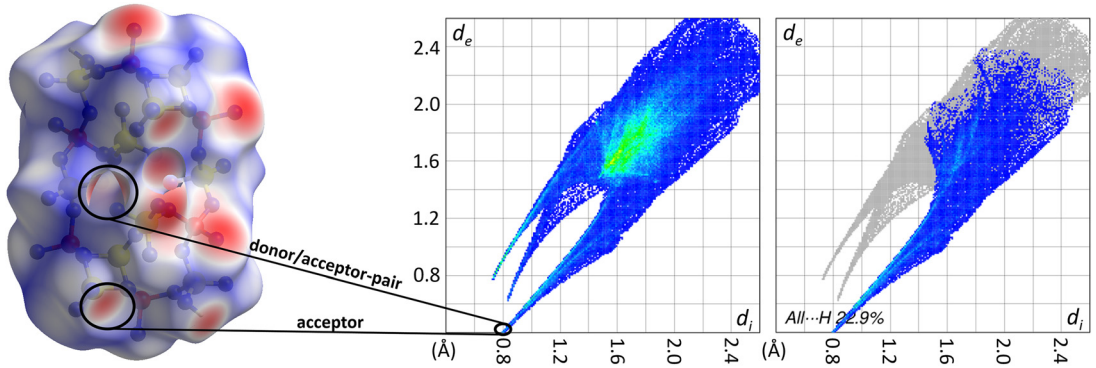

Fig. 6 Hirshfeld-surface mapped with d_{norm} around one zwölfer ring viewed along the stacking direction in the structure of $H_2[B_2(SO_4)_4]$ (left, the same excerpt is shown in Fig. 7 left). Full fingerprint plot of the surface (top-right) and fingerprint plot delineated into the contacts to exterior H-atoms (bottom-right) contributing to 22.9% of the surface area.

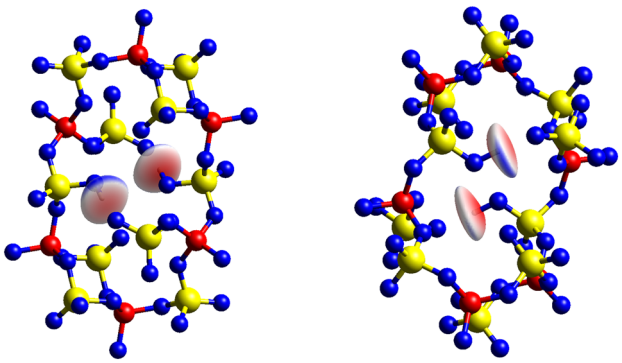

Fig. 7 Hirshfeld-surfaces mapped with d_{norm} around both crystallographically independent H-atom positions inside their respective ring structures H1 on the left and H2 on the right; blue – oxygen, red – boron, yellow – sulfur.

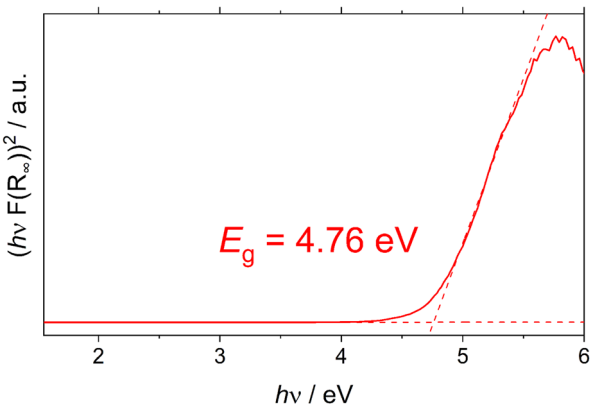

Fig. 8 Tauc plot calculated from the UV-Vis spectrum of $Cd[B_2(SO_4)_4]$ shown in Fig. S14† assuming a direct band gap.

and β-$Mg[B_2(SO_4)_4]$. The S–O stretching modes appear between 1400 and 1300 cm^{-1} and around 1200 cm^{-1}. The subsequent bands between 1180 cm^{-1} and 850 cm^{-1} can be assigned to $\nu_{asym/sym}$ (B–O) and ν_{sym} (S–O). Below, the spectrum is governed by bending vibrations, namely the asymmetric bending vibrations δ_{asym} (O–S–O, O–B–O, S–O–B) between 720 cm^{-1} and 435 cm^{-1} and δ_{asym} (O–S–O, S–O–Cd) below.

UV-Vis spectroscopy. The powder reflectance spectrum of $Cd[B_2(SO_4)_4]$ is shown in Fig. S14.† It is governed by the fundamental absorption due to the bandgap of the sample in the UV regime since there are no valence d electrons in Cd^{2+}. The optical band gap was estimated using the Tauc plot in Fig. 8 with an experimental value of 4.76(1) eV.

Thermal analysis

The thermal decomposition of $Cd[B_2(SO_4)_4]$ was investigated by thermogravimetric analysis (TGA) under nitrogen atmosphere and temperature-programmed powder X-ray diffraction (TPXRD) inside a sealed argon filled glass capillary. According to the results of the former (Fig. 9), $Cd[B_2(SO_4)_4]$ decomposes above 330 °C *via* a two-step process. After the first step, amorphous B_2O_3 and $CdSO_4$ are formed. In turn, the latter decomposes starting at 850 °C to CdO. These steps are accompanied by the evaporation of three moles SO_3 and one SO_3, respect-

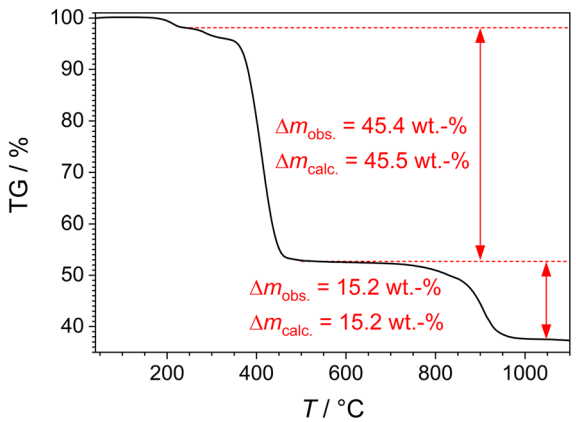

Fig. 9 Thermogravimetric analysis of $Cd[B_2(SO_4)_4]$: prior to the decomposition of $Cd[B_2(SO_4)_4]$, adhesive sulfuric acid evaporates resulting in the small step below 300 °C.

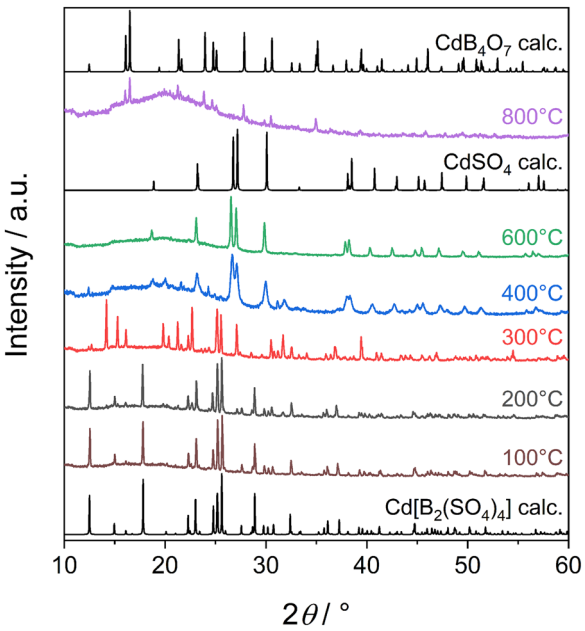

Fig. 10 TPXRD patterns of $Cd[B_2(SO_4)_4]$ compared to calculated patterns for $Cd[B_2(SO_4)_4]$ from SC-XRD, $CdSO_4$ [54] and CdB_4O_7;[55] details are discussed in the text.

ively. The last step is in accordance with earlier reports on the thermal decomposition of $CdSO_4$.[51] Additionally, the decomposition process was investigated by TPXRD (Fig. 10) confirming the formation of $CdSO_4$ and showing the formation of CdB_4O_7 at 800 °C – by the reaction of CdO and B_2O_3. This behaviour is well-known for borosulfates.[15,52] Gravimetrically, it is not possible to discriminate between mixtures of CdO and B_2O_3, and of CdO and CdB_4O_7. Measurements at higher temperatures close to the melting point of CdB_4O_7 (976 °C)[53] resulted in a loss of crystallinity presumably accompanied by glass formation. This also explains why no PXRD could be measured using the residue from the TGA measurement. Additionally, a sample of $Cd[B_2(SO_4)_4]$ heated for 10 h at 1000 °C in a corundum crucible inside a tube furnace could not be separated from the crucible after the heat treatment – presumably due to the same reason. Interestingly, a novel pattern was observed at 300 °C (Fig. 10). This is related to the formation of simultaneously reported $Cd[B_2O(SO_4)_3]$.[34] A more detailed description of the complex thermal decomposition of these cadmium borosulfates is given in the respective publication.

Experimental section

Syntheses

$H_2[B_2(SO_4)_4]$. To synthesize $H_2[B_2(SO_4)_4]$, the generation of SO_3 is essential. However, SO_3 is an extreme oxidizer and needs careful handling. Furthermore, it is very moisture sensitive. Thus, we used a specially designed glass apparatus and procedure that allows for a reaction under complete exclusion of air.

To synthesize the acid, H_3BO_3 (200 mg, Carl Roth, 99.8%) was placed a thick-walled glass ampoule (length 300 mm, outer diameter 16 mm, wall thickness 1.8 mm) and attached to an apparatus for the generation of SO_3. The latter has been conducted under strictly inert atmosphere. To generate SO_3, oleum (Sigma-Aldrich, 20% SO_3) was added carefully to an excessive amount P_4O_{10} (Merck, 97%). In the following, the mixture was heated to 130 °C *via* an oil bath. Thus, SO_3 was transferred to the gaseous phase. Above the dropping funnel a Teflon®-lined manometer has been used to monitor the pressure. SO_3 accumulates in a burette, which is part of the specially designed apparatus. The burette is accessible after opening a Teflon®-lined valve. Eventually, liquid SO_3 has been added dropwise to the attached ampoule *via* utilization of the burette. For the synthesis of $H_2[B_2(SO_4)_4]$ an amount of 0.4 ml SO_3 is needed. Additionally, the ampoule was torch sealed under reduced pressure and placed in a box furnace. The ampoule was heated to 393 K from 298 K with a heating rate of 0.07 K min^{-1}. The temperature was maintained for 48 h and finally reduced to 298 K with a cooling rate of 0.02 K min^{-1}.

$Cd[B_2(SO_4)_4]$. *Via* synthesis **I**, 86.1 mg CdO (Fluka, 99%), 300 mg H_3BO_3 (Carl Roth, 99.8%) and 1 ml oleum (Sigma-Aldrich, 65% SO_3) were loaded into a thick-walled glass ampoule (length 300 mm, outer diameter 16 mm, wall thickness 1.8 mm). The ampule was torch-sealed under reduced pressure and placed in a box furnace. The ampoule was heated to 523 K from 298 K with a heating rate of 1.67 K min^{-1}. The temperature was maintained for 96 h and eventually reduced to 298 K with a cooling rate of 0.04 K min^{-1}.

For synthesis **II**, 0.5 mmol CdO (Fluka, 99%) and 1.25 mmol B_2O_3 (Sigma-Aldrich, 99%) were ground together, and loaded into a silica glass ampoule (length 150 mm, outer diameter: 12 mm, wall thickness: 1 mm) together with 1 ml oleum (VWR, 65% SO_3). Subsequently, the ampoule was fused under ambient pressure and placed in a muffle furnace applying the following temperature program: heating to 573 K with a heating rate of 100 K h^{-1}, holding the temperature for 60 h, and cooling down to room temperature with a cooling rate of 100 K h^{-1}.

The ampoules were opened after cooling with liquid nitrogen (**Caution:** During and even after the reaction the ampoules are under remarkable pressure and must therefore be handled with care). After decantation of the excess sulfuric acid, the Entweder weglassen oder Summenformel samples were washed with 5 ml anhydrous acetonitrile (Acros, 99.9%, extra dry) using a frit in a Schlenk line under nitrogen atmosphere. Afterwards, the product were transferred into an argon filled glovebox. The product is sensitive towards moisture and hence was stored under inert conditions for further investigations. Even minimal quantities of H_2O lead to the degradation of $Cd[B_2(SO_4)_4]$ towards $CdSO_4 \cdot H_2O$ (Fig. S15†).

Single-crystal structure determination

Immediately after opening the ampoules, single-crystals were taken directly out of the mother liquor and transferred into inert oil. Suitable single-crystals were selected under a polarizing microscope, mounted onto a glass needle (∅ = 100 μm) or

a MicroLoop (MiTeGen, ∅ = 50 μm) and immediately placed into a stream of cold nitrogen inside the diffractometer. Diffraction data were collected with Bruker D8 Quest κ and Bruker D8 Venture diffractometers using Mo-K_α radiation (λ = 0.71073 Å). Absorption correction was performed by the multi-scan method. The structures were solved by direct methods difference Fourier techniques and refined by full-matrix least-squares technique with the SHELXL crystallographic software package.[56] Anisotropic refinement was performed for all non-hydrogen atoms. The hydrogen atoms were refined freely using residual density of electrons for localization. Relevant crystallographic data and further details of the structure determinations are summarized in Tables S2 and 13.†

Further details of the crystal structure investigations may be obtained at **https://www.ccdc.cam.ac.uk/** on quoting the depository numbers CCDC-2207483 ($H_2[B_2(SO_4)_4]$), CCDC-2176209, CCDC-2171676 ($Cd[B_2(SO_4)_4]$), the names of the authors, and citation of this publication. CCDC-2176209 gives the data measured at 173(2) K, whereas CCDC-2171676 gives the data for a measurement at 250(2) K. The latter was also used for the discussion in the main manuscript, if not stated otherwise.

X-ray powder diffraction

The samples were ground and filled into glass capillaries (outer diameter 0.7 mm or 0.3 mm, wall thickness 0.01 mm) inside an argon filled glovebox. The data were collected – both in transmission geometry – with a Stoe Stadi P powder diffractometer with Ge(111)-monochromatized Mo-$K_{\alpha1}$-radiation (λ = 0.7093 Å) and a Dectris Mythen 1K detector, and Bruker D8 Advance diffractometer with Cu-K_α radiation (λ = 1.5418 Å) with a 1D LynxEye detector, steps of 0.02°, generator driven at 40 kV and 40 mA, respectively. For the latter instrument, the higher background at lower diffraction angles is due to the absorption of the glass capillary.

Temperature-programmed X-Ray powder diffraction (TPXRD) was performed with the latter device using a furnace attachment and a silica-glass Hilgenberg capillary (outer diameter 0.3 mm, wall thickness 0.01 mm). The additional background between $12.5° < 2\theta < 30°$ is due to the used furnace attachment.

Rietveld refinement

Analysis of diffraction data was performed using the Rietveld method with the programs Topas 4.2 [57] and TOPAS 5,[58] respectively. The instrumental resolution function was determined empirically from a set of fundamental parameters using a reference scan of Si (NIST 640d).[59] The structural model from our single-crystal XRD measurement was used as a starting model for Rietveld analysis. The isotropic displacement parameters were constrained to one common value for all atoms in order to minimize quantification errors. Details are displayed in Fig. S5 and S6 as well as Table S1.†

Hirshfeld-surface analysis

To calculate the Hirshfeld-surfaces, the CrystalExplorer 21.2 [50] program-package was used. All hydrogen bonds lengths were set to normalized values (0.983 Å for O–H) by the program prior to the calculation. The electron densities for each atom type were taken from the basis sets calculated by Koga *et al.*[60] and the surfaces were generated on the very high setting for the number of grid points.

FTIR spectroscopy

The ground sample was mixed with KBr in a roughly 1 : 10 ratio and pressed with a pressure apparatus with a set pressure of 0.6 tons. The thin and slightly transparent pellet was placed into a BRUKER Alpha II FT-IR-Spectrometer. Scans were performed in a range from 360 cm^{-1} to 4000 cm^{-1}, with a resolution of 2 cm^{-1} and 90 scans per sample. Background corrections were applied by measuring a pure KBr pellet. The used program was Opus version 8.[61]

UV-Vis spectroscopy

The UV-Vis spectrum was recorded as diffuse reflection spectrum at room temperature with a Varian Cary 300 Scan UV-Vis spectrophotometer using an Ulbricht sphere detector and a deuterium lamp/tungsten–halogen lamp light source (scan range: 200–800 nm, increment 1 nm, scan rate: 120 nm min^{-1}).

Thermal analysis

The thermogravimetric analysis (TGA) was performed with a NETZSCH STA 409 PC Luxx thermobalance under nitrogen atmosphere with 70 mL min^{-1} flow in alumina crucibles (heating rate: 10 K min^{-1}).

Conclusions

Multiple transition metal borosulfates with the general sum formula $M[B_2(SO_4)_4]$ are known comprising phyllosilicate-analogous anionic substructures formed by adjacent zwölfer and vierer rings. In this contribution, the "parent" acid $H_2[B_2(SO_4)_4]$ is presented and another member, namely $Cd[B_2(SO_4)_4]$, is added to the aforementioned group. The hydrogen bonding situation in $H_2[B_2(SO_4)_4]$ occurs solely within the zwölfer rings, *i.e.* within the borosulfate layer. This and the resulting distortion of these rings could be described in detail by Hirshfeld-surface analysis. $Cd[B_2(SO_4)_4]$ can be described as the cadmium salt of the heteropolyacid $H_2[B_2(SO_4)_4]$. It adapts the $Mn[B_2(SO_4)_4]$ structure type with "cation within layers" configuration. Further, the optical properties investigated by infrared and UV-Vis spectroscopy are in line with the X-ray diffraction results and revealed an optical band gap of 4.76 eV using a Tauc plot. Thermally, $Cd[B_2(SO_4)_4]$ decomposes at 330 °C *via* a two-step process to CdO and B_2O_3. In future experiments, we will elucidate if the acid can be used directly to synthesize the respective phyllosilicate-analogous metal borosulfates.

Author contributions

M. H. prepared $Cd[B_2(SO_4)_4]$, solved its crystal structure and did the characterization by UV-Vis spectroscopy and the thermal analysis, and wrote parts of the original

draft. L. C. P. independently prepared $Cd[B_2(SO_4)_4]$, solved its crystal structure and did the characterization *via* IR spectroscopy, and wrote parts of the original draft. S. S. did the experiments on $H_2[B_2(SO_4)_4]$, conducted the Hirshfeld analysis and wrote parts of the original draft. H. H. and J. B. supervised the work by L. C. P., H. A. H. supervised the work by M. H. and wrote parts of the original draft. J. B. supervised the work by S. S., prepared the first sample of $H_2[B_2(SO_4)_4]$ and wrote parts of the original draft. All authors reviewed and edited the final draft of the manuscript.

Conflicts of interest

There are no conflicts to declare.

Acknowledgements

J. B. thanks the Fonds der Chemischen Industrie (FCI) and the Max-Buchner-Forschungsstiftung for financial support. H. A. H. and M. H. thank the Deutsche Forschungsgemeinschaft (DFG) for financial support under the project HO 4503/5-1. The authors thank Assoc. Univ.-Prof. Dr. Gunter Heymann (University Innsbruck) for the measurement of the crystal structure of $H_2[B_2(SO_4)_4]$. L. C. P. is grateful for the PhD scholarship of the University of Innsbruck.

References

1 J. Bruns, H. A. Höppe, M. Daub, H. Hillebrecht and H. Huppertz, *Chem. – Eur. J.*, 2020, **26**, 7966–7980.
2 M. Hämmer, L. Bayarjargal and H. A. Höppe, *Angew. Chem., Int. Ed.*, 2021, **60**, 1503–1506, (*Angew. Chem.*, 2021, **133**, 1525–1529).
3 Y. Li, Z. Zhou, S. Zhao, F. Liang, Q. Ding, J. Sun, Z. Lin, M. Hong and J. Luo, *Angew. Chem., Int. Ed.*, 2021, **60**, 11457–11463.
4 Z. Li, W. Jin, F. Zhang, Z. Chen, Z. Yang and S. Pan, *Angew. Chem., Int. Ed.*, 2022, e202112844.
5 P. Netzsch, R. Stroh, F. Pielnhofer, I. Krossing and H. A. Höppe, *Angew. Chem., Int. Ed.*, 2021, **60**, 10643–10646, (*Angew. Chem.*, 2021, **133**, 10738–10741).
6 L. C. Pasqualini, H. Huppertz, M. Je, H. Choi and J. Bruns, *Angew. Chem., Int. Ed.*, 2021, **60**, 19740–19743, (*Angew. Chem.*, 2021, **133**, 19892–19896).
7 H. A. Höppe, K. Kazmierczak, M. Daub, K. Förg, F. Fuchs and H. Hillebrecht, *Angew. Chem., Int. Ed.*, 2012, **51**, 6255–6257.
8 M. Daub, K. Kazmierczak, P. Gross, H. Höppe and H. Hillebrecht, *Inorg. Chem.*, 2013, **52**, 6011–6020.
9 M. Daub, H. A. Höppe and H. Hillebrecht, *Z. Anorg. Allg. Chem.*, 2014, **640**, 2914–2921.
10 J. Bruns, M. Podewitz, O. Janka, R. Pöttgen, K. Liedl and H. Huppertz, *Angew. Chem.*, 2018, **130**, 9548–9552, (*Angew. Chem.*, 2018, **130**, 9693–9697).
11 M. Daub, K. Kazmierczak, H. A. Höppe and H. Hillebrecht, *Chem. – Eur. J.*, 2013, **19**, 16954–16962.
12 J. Bruns, M. Podewitz, M. Schauperl, K. Liedl, O. Janka, R. Pöttgen and H. Huppertz, *Eur. J. Inorg. Chem.*, 2017, 3981–3989.
13 S. Schönegger, J. Bruns, B. Gartner, K. Wurst and H. Huppertz, *Z. Anorg. Allg. Chem.*, 2018, **644**, 1702–1706.
14 P. Netzsch and H. A. Höppe, *Z. Anorg. Allg. Chem.*, 2020, **646**, 1563–1569.
15 P. Netzsch, P. Gross, H. Takahashi and H. A. Höppe, *Inorg. Chem.*, 2018, **57**, 8530–8539.
16 J. Bruns, M. Podewitz, M. Schauperl, B. Joachim, K. Liedl and H. Huppertz, *Chem. – Eur. J.*, 2017, **23**, 16773–16781.
17 L. C. Pasqualini, O. Janka, S. Olthof, H. Huppertz, K. Liedl, M. Podewitz and J. Bruns, *Chem. – Eur. J.*, 2020, **26**, 17405–17415.
18 P. Netzsch, F. Pielnhofer, R. Glaum and H. A. Höppe, *Chem. – Eur. J.*, 2020, **26**, 14745–14745.
19 W. Loewenstein, *Am. Mineral.*, 1954, **39**, 92–96.
20 L. Pauling, *J. Am. Chem. Soc.*, 1929, **51**, 1010–1026.
21 P. Gross, A. Kirchhain and H. A. Höppe, *Angew. Chem., Int. Ed.*, 2016, **55**, 4353–4355, (*Angew. Chem.*, 2016, **128**, 4426–4428).
22 C. Logemann and M. S. Wickleder, *Angew. Chem., Int. Ed.*, 2013, **52**, 14229–14232, (*Angew. Chem.*, 2013, **125**, 14479–14482).
23 M. Daub and H. Hillebrecht, *Eur. J. Inorg. Chem.*, 2015, 4176–4181.
24 P. Netzsch, P. Gross, H. Takahashi, S. Lotfi, J. Brgoch and H. A. Höppe, *Eur. J. Inorg. Chem.*, 2019, 3975–3981.
25 M. Daub, H. A. Höppe and H. Hillebrecht, *Z. Anorg. Allg. Chem.*, 2014, **640**, 2914–2921.
26 P. Netzsch and H. A. Höppe, *Inorg. Chem.*, 2020, **59**, 18102–18108.
27 P. Netzsch and H. A. Höppe, *Eur. J. Inorg. Chem.*, 2021, **11**, 1065–1070.
28 S. Sutorius, D. van Gerven, S. Olthof, B. Rasche and J. Bruns, *Chem. – Eur. J.*, 2022, e202200004.
29 J. Bruns, M. Podewitz, M. Schauperl, B. Joachim, K. Liedl and H. Huppertz, *Chem. – Eur. J.*, 2017, **23**, 16773–16781.
30 L. C. Pasqualini, H. Huppertz and J. Bruns, *Inorganics*, 2019, **7**, 145–154.
31 M. Hämmer, F. Pielnhofer, O. Janka, H. Takahashi, P. Gross, R. Pöttgen and H. A. Höppe, *Dalton Trans.*, 2022, **51**, 3104–3115.
32 R. J. Gillespie and E. A. Robinson, *Can. J. Chem.*, 1962, **40**, 784–787.
33 G. Schott and H. U. Kibbel, *Z. Anorg. Allg. Chem.*, 1962, **314**, 104–112.
34 M. Hämmer and H. A. Höppe, *Z. Anorg. Allg. Chem.*, 2022, e202200197.
35 T. Steiner, *Angew. Chem., Int. Ed.*, 2002, **41**, 48–76, (*Angew. Chem.*, 2002, **114**, 50–80).
36 T. Balić Žunić and E. Makovicky, *Acta Crystallogr., Sect. B: Struct. Sci.*, 1996, **52**, 78–81.
37 E. Makovicky and T. Balić-Žunić, *Acta Crystallogr., Sect. B: Struct. Sci.*, 1998, **54**, 766–773.
38 H. A. Höppe, *J. Solid State Chem.*, 2009, **182**, 1786–1791.
39 T. Kato and Y. Takeuchi, *Can. Mineral.*, 1983, **21**, 1–6.

40 R. D. Shannon, *Acta Crystallogr., Sect. A: Cryst. Phys., Diffr., Theor. Gen. Crystallogr.*, 1976, **32**, 751–767.
41 M. Hämmer, J. Müller and H. A. Höppe, unpublished results.
42 D. W. Smith, *J. Chem. Educ.*, 1987, **64**, 480–481.
43 R. Hoppe, *Angew. Chem.*, 1966, **78**, 52–63.
44 R. Hoppe, *Angew. Chem., Int. Ed. Engl.*, 1970, **9**, 25–34, (*Angew. Chem.*, 1970, **82**, 7–16).
45 R. Hoppe, *Z. Kristallogr.*, 1979, **150**, 23–52.
46 R. Hübenthal, *MAPLE. Program for the Calculation of the Madelung Part of Lattice Energy*, Universität Gießen, Gießen, 1993.
47 D. Casanova, J. Cirera, M. Llunell, P. Alemany, D. Avnir and S. Alvarez, *J. Am. Chem. Soc.*, 2004, **126**, 1755–1763.
48 M. Llunell, D. Casanova, J. Cirera, P. Alemany and S. Alvarez, *SHAPE 2.1*, Univ. Barcelona, Barcelona, Spain.
49 M. A. Spackman and D. Jayatilaka, *CrystEngComm*, 2009, **11**, 19–32.
50 P. R. Spackman, M. J. Turner, J. J. McKinnon, S. K. Wolff, D. J. Grimwood, D. Jayatilaka and M. A. Spackman, *J. Appl. Crystallogr.*, 2021, **54**, 1006–1011.
51 H. Tagawa and K. Kawabe, *Thermochim. Acta*, 1990, **158**, 293–302.
52 P. Netzsch, M. Hämmer, P. Gross, H. Bariss, T. Block, L. Heletta, R. Pöttgen, J. Bruns, H. Huppertz and H. A. Höppe, *Dalton Trans.*, 2019, **48**, 4387.
53 T. N. Khamaganova, T. G. Khumaeva, A. K. Subanakov and A. V. Perevalov, *Inorg. Mater.*, 2017, **53**, 81–85.
54 K. Aurivillius and C. Stålhandske, *Z. Kristallogr.*, 1980, **153**, 121–129.
55 M. Ihara and J. Krogh-Moe, *Acta Crystallogr.*, 1966, **20**, 132–134.
56 G. M. Sheldrick, *Acta Crystallogr., Sect. C: Struct. Chem.*, 2015, **71**, 3–8.
57 *TOPAS4.2*, Bruker, Karlsruhe, Germany, 2009.
58 *Bruker AXS, Topas V5, General profile and structure analysis software for powder diffraction data. User's Manual*, Karlsruhe, Germany, 2014.
59 R. W. Cheary, A. A. Coelho and J. P. Cline, *J. Res. Natl. Inst. Stand. Technol.*, 2004, **109**, 1–25.
60 T. Koga, K. Kanayama, T. Watanabe, T. Imai and A. J. Thakkar, *Theor. Chem. Acc.*, 2000, **104**, 411–413.
61 OPUS version 8.2 build 8, 2, 28 (20190310) Copyright© Bruker Optic GmbH.